PERGAMON

International Journal of Solids and Structures 40 (2003) 1311–1327

INTERNATIONAL JOURNAL OF SOLIDS and STRUCTURES

www.elsevier.com/locate/ijsolstr

A semi-analytical buckling analysis of imperfect cylindrical shells under axial compression

M. Jamal [a], L. Lahlou [a], M. Midani [a], H. Zahrouni [b], A. Limam [c], N. Damil [a], M. Potier-Ferry [b,*]

[a] *Faculté des sciences Ben M'Sik, Laboratoire de Calcul Scientifique en Mécanique, Université Hassan II—Mohammedia, B.P. 7955, Sidi Othman, Casablanca, Morocco*

[b] *LPMM, UMR CNRS 7554, ISGMP, Université de Metz, Ile du Saulcy, 57045 Metz Cedex 01, France*

[c] *INSA Lyon, URGC—Structures, Bât. 304-20, avenue Albert Einstein, 69621 Villeurbanne Cedex, France*

Received 6 June 2000; received in revised form 26 September 2002

Abstract

In the framework of the cellular bifurcation theory, we investigate the effect of distributed and/or localized imperfections on the buckling of long cylindrical shells under axial compression. Using a double scale perturbative approach including modes interaction, we establish that the evolution of amplitudes of instability patterns is governed by a non-homogeneous second order system of three non-linear complex equations. The localized imperfections are included by employing jump conditions for their amplitude and permitting discontinuous derivatives. By solving these amplitude equations, we show the influence of distributed and/or localized imperfections on the reduction of the critical load. To assess the validity of the present method, our results are compared to those given by two finite element codes.

Keywords: Buckling; Cylindrical shells; Axial compression; Imperfections; Double scale method; Cellular bifurcation

1. Introduction

In this paper, we present a semi-analytical method to compute the reduction of the buckling load of cylindrical shells under axial compression in presence of distributed and/or localized imperfections by coupling a double scale asymptotic analysis in the axial direction and a Fourier harmonic formulation using only three modes in the circumferential direction.

The buckling phenomena of imperfect cylindrical shells is one of the most challenging problems of the theory of elastic stability. A considerable amount of research has been undertaken to clarify this problem. A very useful bibliography can be found in the works of Arbocz et al. (1987), Brush and Almroth (1975), Budiansky and Hutchinson (1966), Bushnell (1985), Dubas and Vandepite (1987), Hunt and Neto (1991), Yamada and Croll (1999) and Yamaki (1984).

* Corresponding author. Tel.: +33-3-87-31-5360; fax: +33-3-87-31-5366.
E-mail address: potier-ferry@lpmm.univ-metz.fr (M. Potier-Ferry).

0020-7683/02/$ - see front matter © 2002 Elsevier Science Ltd. All rights reserved.
PII: S0020-7683(02)00583-8

In the post-buckling analysis of structures with a large ratio aspect, the instability patterns are often featured by a cellular (or diamond) shape with a large number of cells (Wesfreid and Zaleski, 1984). In the case of cellular instability in an unbounded domain, the linear analysis leads to a continuous spectrum. The classical stability theory (Budiansky, 1974; Koiter, 1945; Potier-Ferry, 1987; Thompson and Hunt, 1973) can be applied provided that, at the bifurcation load, the eigenspace is of finite dimension: in this case, the Lyapounov–Schmidt method gives an algebraic equation which leads to a reduction of critical load proportional to $(a_0)^{2/3}$ in presence of a distributed imperfection of amplitude a_0. However, in the case of cellular bifurcation, the buckling modes are nearly coincident and the number of modes is large.

Thus the classical algebraic amplitude equation is replaced by a complex differential equation which permits to account for the spatial variations of the amplitude of the post-buckling patterns (Newell and Whitehead, 1969; Segel, 1969). The localized imperfection sensitivity was studied theoretically via several asymptotic analysis (Abdelmoula et al., 1992; Amazigo et al., 1970; Amazigo and Fraser, 1971; Damil and Potier-Ferry, 1992). In their work, Amazigo et al. (1970) have established for a beam buckling problem that the first derivative of the amplitude of buckling pattern is discontinuous in the region where the localized imperfection is significant and the reduction of critical load follows a linear law.

In an earlier paper Jamal et al. (1999) have studied the effect of localized imperfection on the buckling of long cylindrical shells under axial compression by using a double scale perturbative method including modal patterns that interact. We have shown that the evolution of amplitudes of buckling patterns is governed by three coupled non-linear differential equations with discontinuous derivatives in the region where the localized imperfections are significant. We have also proved that the reduction of critical load follows a two-third power law (i.e. proportional to $(a_1)^{2/3}$, where a_1 is the amplitude of localized imperfection).

The aim of this work is to extend the previous procedure, as in Jamal et al. (1999), to study the stability of long cylindrical shells subjected to an axial compression under the presence of both distributed and localized imperfections. Following the same method as in Jamal et al. (1999), a second order differential system of non-homogeneous coupled non-linear equations with discontinuous derivatives is found. The influence of these two types of imperfections and their interaction is studied. The problem is reduced to numerically solving three non-homogenous, coupled non-linear equations.

2. Post-buckling problem for imperfect cylindrical shells

We consider a long circular cylindrical shell of radius, R, length, L and thickness, h, which is made of an homogeneous, isotropic elastic material with Young's modulus, E and Poisson's ratio, v; it is subjected to an axial compressive load P. The coordinate system is shown in Fig. 1 and the displacement components will be denoted by u, v and w. Within the Donnell theory and if the pre-buckling rotations are neglected, in the presence of an initial displacement $d(x,y)$, the transverse displacement $w(x,y)$ and the additional stress function $\phi(x,y)$ are solutions of

$$k^2\nabla^4 w + \lambda\left(\frac{\partial^2 w}{\partial x^2} + \frac{\partial^2 d}{\partial x^2}\right) - \rho\frac{\partial^2 \phi}{\partial x^2} = [w+d,\phi] \tag{1}$$

$$\nabla^4\phi + \rho\frac{\partial^2 w}{\partial x^2} = -\frac{1}{2}[w+d, w+d] \tag{2}$$

where $\lambda = P/Eh$ is the load parameter, $k^2 = h^2/12(1-v^2)$ and $\rho = 1/R$ is the shell curvature. The stress function ϕ is related to the resultant stress as follows:

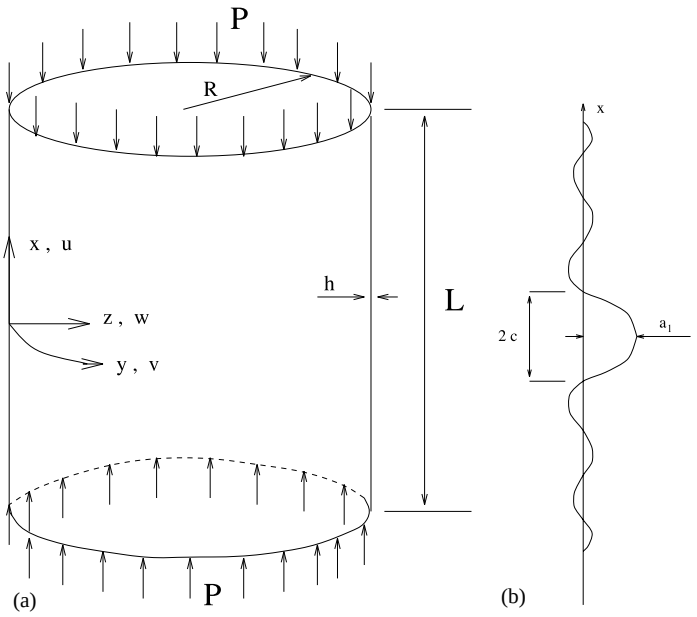

Fig. 1. (a) Geometrical description, (b) localized imperfection.

$$N_x = Eh\frac{\partial^2\phi}{\partial y^2}, \quad N_y = Eh\frac{\partial^2\phi}{\partial x^2}, \quad N_{xy} = -Eh\frac{\partial^2\phi}{\partial x\partial y} \tag{3}$$

∇^4 denotes the biharmonic operator, and $[\cdot,\cdot]$ is the usual bracket operator:

$$[g,f] = \frac{\partial^2 g}{\partial x^2}\frac{\partial^2 f}{\partial y^2} + \frac{\partial^2 g}{\partial y^2}\frac{\partial^2 f}{\partial x^2} - 2\frac{\partial^2 g}{\partial x\partial y}\frac{\partial^2 f}{\partial x\partial y} \tag{4}$$

We denote the initial imperfection as follows:

$$d(x,y) = a_{\mathrm{l}}g_{\mathrm{l}}(x,y) + a_{\mathrm{r}}g_{\mathrm{r}}(x,y) \tag{5}$$

where a_i and g_i are the amplitude and the shape of the localized ($i = \mathrm{l}$) or the distributed ($i = \mathrm{r}$) imperfections. In addition, we suppose that $g_{\mathrm{l}}(x,y)$ is rapidly reducing for large $|x|$ (Fig. 1b). Within the standard linear theory, the critical value of the load λ is characterized by the existence of a buckling mode (w,ϕ), which is the solution of the linearized equations without initial imperfections. Because the aspect ratio is large, the boundary conditions at the ends of the shell are replaced by the requirement of a harmonic behaviour in the x-direction. The whole buckling modes can be expressed as:

$$w = A\exp(\mathrm{i}\gamma x)\cos(\beta\gamma y) + \text{c.c.} \tag{6}$$

$$\phi = \frac{\rho A}{\gamma^2(1+\beta^2)^2}\exp(\mathrm{i}\gamma x)\cos(\beta\gamma y) + \text{c.c.} \tag{7}$$

$$\lambda = k^2\gamma^2(1+\beta^2)^2 + \frac{\rho^2}{\gamma^2(1+\beta^2)^2} \tag{8}$$

where A is a complex constant, $\beta\gamma = \rho n$, n is the wave number in the circumferential direction, β is the modal aspect ratio (axial/circumferential wavelength), and c.c. denotes the complex conjugate. The

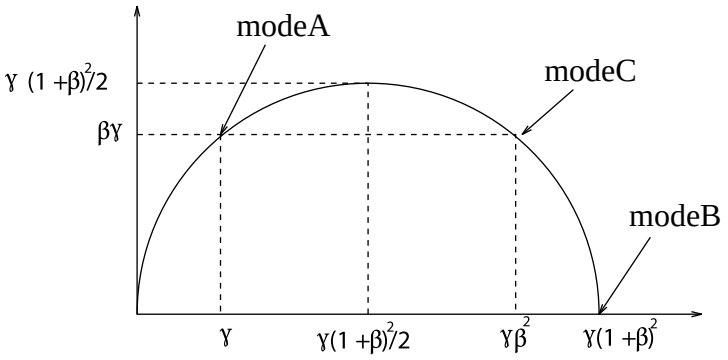

Fig. 2. The Koiter circle.

minimization of (8) gives the classical critical load $\lambda_c = 2\rho k$. All the modes corresponding to this load are those on the Koiter circle (Fig. 2). The relation: $\gamma^2(1+\beta^2)^2 = \rho/k$ is the required condition for the mode (6) to be on the Koiter circle.

3. Three coupled amplitude equations: post-buckling analysis

We solve the non-linear differential problem (Eqs. (1) and (2)) by using a double scale perturbation analysis (Newell and Whitehead, 1969; Segel, 1969). The expansion parameter η is connected to the amplitudes of imperfection a_l and a_r (see Damil and Potier-Ferry, 1992) by:

in the case of distributed imperfection

$$\eta = (a_r)^{1/2} \tag{9}$$

and in the case of localized imperfection

$$\eta = (a_l)^{2/3} \tag{10}$$

To account for both distributed and localized imperfections, the two small parameters a_r and a_l are replaced by three parameters t_1, t_2 and η:

$$a_r = t_1\eta^2 \tag{11}$$

and

$$a_l = t_2\eta^{3/2} \tag{12}$$

where only η is small. If $t_1 = 1$, t_2 represents a ratio between the two types of imperfections:

$$t_2 = \frac{a_l}{(a_r)^{3/4}} \tag{13}$$

If t_2 is large (respectively small), the only localized (respectively distributed) imperfection is significant. If t_2 is of order of unity, both imperfections must be taken into account. In order to obtain not only periodic solutions, we use the classical double scale expansion method to analyse cellular bifurcation (Newell and Whitehead, 1969; Potier-Ferry, 1983; Segel, 1969). Following the same method as in Jamal et al. (1999), we introduce the slow space variable X which is connected to the rapid variable x by

$$X = \eta^{1/2}x \tag{14}$$

We assume that the unknown

$$u = (w, \phi) \tag{15}$$

is a function of the three "independent" variables X, x, y. According to the classical rule within the double scale expansion method, the following identities hold (for $n = 1, 2, \ldots$):

$$\frac{\partial^m}{\partial x^m} \to \sum_{p=0}^{m} C_m^p \eta^{(m-p)/2} \frac{\partial^p}{\partial x^p} \frac{\partial^{m-p}}{\partial X^{m-p}}, \quad C_m^p = \frac{m!}{p!(m-p)!} \tag{16}$$

where $\partial^0/\partial X^0 = \partial^0/\partial x^0 = 1$. By employing the classical rule, the unknown u and the load parameter λ are searched in series expansion form with respect to η:

$$u(x, X, y) = \eta u_1(x, X, y) + \eta^{3/2} u_{3/2}(x, X, y) + \eta^2 u_2(x, X, y) + \cdots \tag{17}$$

$$\lambda - \lambda_c = \eta\lambda_1 + \eta^{3/2}\lambda_{3/2} + \eta^2\lambda_2 + \cdots \tag{18}$$

Substituting (16)–(18) into the equilibrium equations (1) and (2), we find the following equations in terms of the first three orders η, $\eta^{3/2}$, η^2:

$$L_\lambda u_1 = 0 \tag{19}$$

$$L_\lambda u_{3/2} = F_{3/2} + G_l \tag{20}$$

$$L_\lambda u_2 = F_2 + G_r \tag{21}$$

where G_r and G_l are expressed as:

$$G_r = \begin{Bmatrix} -\lambda_c t_1 \frac{\partial^2 g_r(x,y)}{\partial x^2} \\ 0 \end{Bmatrix} \tag{22}$$

$$G_l = \begin{Bmatrix} -\lambda_c \frac{\partial^2 g_l(x,y)}{\partial x^2} \\ 0 \end{Bmatrix} \tag{23}$$

The same linear operator L_λ is employed for the three orders. It is written in the following form:

$$L_\lambda(\cdot) = \begin{bmatrix} k^2\nabla^4 \cdot + \lambda_c \frac{\partial^2 \cdot}{\partial x^2} & -\rho \frac{\partial^2 \cdot}{\partial x^2} \\ \rho \frac{\partial^2 \cdot}{\partial x^2} & \nabla^4 \cdot \end{bmatrix} \tag{24}$$

The right-hand sides (20) and (21) depend on the deflections and stress components w_i and ϕ_i ($i = 1, 3/2$). The expressions of $F_{3/2}$ and F_2 are functions of u_1 and $u_{3/2}$. The vectors G_l and G_r, appearing respectively in Eqs. (20) and (21), are due to the shape of the localized and distributed imperfections.

Following the same procedure as in Jamal et al. (1999), we search for the perturbative equations (19)–(21), solutions taking into account mode interactions. Hence the solution of the first-order equation (19) is taken in the form:

$$u_1 = \begin{Bmatrix} A(X)\exp(i\gamma x)\cos\beta\gamma y + B(X)\exp(i\gamma(1+\beta^2)x) + C(X)\exp(i\beta^2\gamma x)\cos\beta\gamma y + \text{c.c.} \\ A_1(X)\exp(i\gamma x)\cos\beta\gamma y + B_1(X)\exp(i\gamma(1+\beta^2)x) + C_1(X)\exp(i\beta^2\gamma x)\cos\beta\gamma y + \text{c.c.} \end{Bmatrix} \tag{25}$$

where $A_1 = kA$, $B_1 = kB$, $C_1 = kC$. All these three modes appear on the Koiter circle, as shown in Fig. 2. At this stage, the complex amplitudes $A(X)$, $B(X)$ and $C(X)$ are arbitrary functions of the slow variable X. With this u_1, the Eq. (20) contains no secular terms and its solution is given by:

$$u_{3/2} = \left\{ \begin{array}{c} 0 \\ d(X)\exp(\mathrm{i}\gamma x)\cos\beta\gamma y + e(X)\exp(\mathrm{i}\gamma(1+\beta^2)x) + f(X)\exp(\mathrm{i}\beta^2\gamma x)\cos\beta\gamma y + \text{c.c.} \end{array} \right\} + u^{\mathrm{l}}_{3/2} \quad (26)$$

where

$$\mathrm{d}(X) = -\frac{\mathrm{i}2k(1-\beta^2)}{\gamma(1+\beta^2)}A'(X), \quad e(X) = \frac{\mathrm{i}2k}{\gamma(1+\beta^2)}B'(X), \quad f(X) = -\frac{\mathrm{i}2k(1-\beta^2)}{\gamma(1+\beta^2)}C'(X) \quad (27)$$

and $u^{\mathrm{l}}_{3/2}$ account for the solution due to localized imperfections. The 'prime' denotes a differentiation with respect to the slow variable X. The operator L_λ is singular. Hence, the non-homogeneous equation (21) has a solution if only if its right-hand side satisfies the solvability conditions

$$\langle F_2 + G_{\mathrm{r}}, v_i^* \rangle = 0 \quad i = 1, 2, 3 \quad (28)$$

where the vectors v_i^* ($i = 1, 2, 3$) belong to the kernel of the adjoint operator L_λ^* of L_λ. Applying these solvability conditions and returning to the unscaled amplitudes $a(x) = \eta A(x)$, $b(x) = \eta B(x)$, $c(x) = \eta C(x)$ and with an unscaled variable x, we obtain the following three non-homogeneous coupled non-linear second order differential equation satisfied by the real amplitudes (for $x \geqslant 0$ in the case of only symmetric solutions):

$$8k^2(1-\beta^2)^2\frac{\mathrm{d}^2a(x)}{\mathrm{d}x^2} + 2(\lambda-\lambda_{\mathrm{c}})a(x) + 6\rho\beta^2 b(x)c(x) = -2a_{\mathrm{r}}\lambda_{\mathrm{c}}d_a \quad (29)$$

$$8k^2(1-\beta^2)^2\frac{\mathrm{d}^2b(x)}{\mathrm{d}x^2} + 2(\lambda-\lambda_{\mathrm{c}})(1+\beta^2)^2 b(x) + 3\rho\beta^2 c(x)a(x) = -2a_{\mathrm{r}}\lambda_{\mathrm{c}}(1+\beta^2)^2 d_b \quad (30)$$

$$8k^2(1-\beta^2)^2\frac{\mathrm{d}^2c(x)}{\mathrm{d}x^2} + 2(\lambda-\lambda_{\mathrm{c}})\beta^4 c(x) + 6\rho\beta^2 a(x)b(x) = -2a_{\mathrm{r}}\lambda_{\mathrm{c}}\beta^4 d_c \quad (31)$$

Here the right-hand sides of (29)–(31) account for distributed imperfections having the following shape:

$$g_{\mathrm{r}}(x,y) = d_a\cos\gamma x\cos\beta\gamma y + d_b\cos\gamma(1+\beta^2)x + d_c\cos\beta^2\gamma x\cos\beta\gamma y \quad (32)$$

where d_a, d_b and d_c are coefficients linked by the relation $d_a + d_b + d_c = 1$. For simplicity, we limit ourselves to the three mode imperfections (32), but the analysis can be extended to any imperfection shape: indeed, because of Eq. (28), an imperfection that is orthogonal to these modes, does not modify the amplitude equations (29)–(31).

Hence Eqs. (29)–(31) govern the evolution of the modulated amplitudes $a(x)$, $b(x)$ and $c(x)$ which take into account the effect of distributed imperfections.

The effects of localized imperfections are now taken into account solving (20). The solution $u^{\mathrm{l}}_{3/2}$ in (26) accounting for localized imperfection satisfies:

$$L_\lambda u^{\mathrm{l}}_{3/2} = G_{\mathrm{l}} \quad (33)$$

To solve this problem, it is convenient to use the Fourier transform. Generally, Eq. (33) has no localized and smooth solution. To overcome this difficulty, we assume that these solutions are discontinuous at $x = 0$, this means that from the point of view of asymptotic analysis, in the case of a localized imperfection, we solve the non-linear problem by using two different expansions of the generalized displacement u or of its derivatives in the region $x < 0$, $X < 0$ and in the region $x > 0$, $X > 0$. Hence, any quantity in these asymptotic expansions can admit the possibility of discontinuities at $x = 0$ and $X = 0$, but the generalized deflection u, slope $\mathrm{d}u/\mathrm{d}x$, moment $\mathrm{d}^2u/\mathrm{d}x^2$ and shear $\mathrm{d}^3u/\mathrm{d}x^3$ must be continuous at $x = 0$ and $X = 0$. These

continuity conditions lead to continuity conditions on the u_n and their derivatives. Then Eq. (33) is written in Fourier spectral space in the form below:

$$L(\omega)\hat{\boldsymbol{u}}^{1}_{3/2}(\omega,y) = S(\omega,y) \tag{34}$$

where

$$L(\omega) = \begin{bmatrix} k^2\left(\omega^2 - \frac{\partial^2}{\partial y^2}\right)^2 - \lambda_c\omega^2 & \rho\omega^2 \\ -\rho\omega^2 & \left(\omega^2 - \frac{\partial^2}{\partial y^2}\right)^2 \end{bmatrix} \tag{35}$$

is the operator of the problem in Fourier space. The right-hand side $S(\omega,y)$ of (34) is a vectorial complex function depending on localized imperfections and the discontinuities of $u^1_{3/2}$ and their derivatives at $x = 0$.

As the operator $L(\omega)$ is singular for $\omega = \gamma$, $\omega = \beta^2\gamma$ and $\omega = \gamma(1+\beta^2)$, then Eq. (34) has a localized solution if and only if its right-hand side satisfies three solvability conditions:

$$\langle S(\omega,y), V_i^* \rangle = 0 \quad (i = 1,2,3) \tag{36}$$

These solvability conditions lead to the following discontinuous derivatives of the envolopes $a(x)$, $b(x)$, $c(x)$ at $x = 0$ (see Jamal et al., 1999):

$$\begin{aligned} a'(0) &= -\frac{\lambda_c\sqrt{2\pi}}{4k^2\pi R(1-\beta^2)^2}a_1\int_0^{2\pi R}\hat{\boldsymbol{g}}(\gamma,y)\cos\beta\gamma y\,\mathrm{d}y \\ b'(0) &= -\frac{\lambda_c\sqrt{2\pi}}{8k^2\pi R}a_1\int_0^{2\pi R}\hat{\boldsymbol{g}}(\gamma(1+\beta^2),y)\,\mathrm{d}y \\ c'(0) &= -\frac{\lambda_c\beta^4\sqrt{2\pi}}{4k^2\pi R(1-\beta^2)^2}a_1\int_0^{2\pi R}\hat{\boldsymbol{g}}(\beta^2\gamma,y)\cos\beta\gamma y\,\mathrm{d}y \end{aligned} \tag{37}$$

Thus the equilibrium equations (1) and (2) are replaced by the three non-homogeneous coupled non-linear differential equations (29)–(31) and the jump relations (37) which allows one to account for spatial variations of the amplitudes and for the influence of localized and distributed imperfections. These equations will be used in the next section to predict the reduction of the critical load.

4. Numerical predictions of the reduced buckling load

It seems that, the amplitude differential equations (29)–(31) have no closed form solutions, as it was the case for one mode analysis (Abdelmoula et al., 1992). Hence, these equations coupled with the boundary conditions (37) have to be solved by a numerical method. Solving this simplified numerical model is much less expansive than solving a complete cylindrical shell model. Nevertheless, in order to establish the range of validity of the amplitude equations (29)–(31), we have carried out such a finite element shell model within the general code Abaqus and within INCA, that is a specific code for shells of revolution.

Finally, we shall present a few results from the simplified model in order to distinguish the influence of various types of coupled imperfections on the buckling strength of the structure.

4.1. Methodology

For the example considered in this study, the geometry is characterized by a radius of 100 mm and a shell thickness of 0.247 mm. Material properties are described by the Young modulus $E = 198\,000$ MPa and the Poisson's ratio $v = 0.3$. Cylinder length is deduced from the Batdorf parameter $Z = L^2\sqrt{1-v^2}/Rh = 1000$,

which leads to $L = 160.9$ mm. For the proposed shell, a linear analysis gives a critical load of $\lambda_c = 2\rho k = h/R\sqrt{3(1-\nu^2)}$ which means that the collapse of the cylindrical shell occurs for a limit pressure of $P_c = Eh\lambda_c = 73.11$ N/mm.

Let us note that this choice of the test geometry and of a large Z is consistent with the linear pre-buckling assumption. We have chosen a large Z because the effects of non-linear pre-buckling rotations is a bit stronger for short specimens and therefore our simplified model is less accurate in the latter case. Probably a simplified model coupling the amplitude equations (29)–(31) with these effects would be too intricate for a result of little significance.

For the critical load P_c, all modes located on the Koiter circle are solutions of the linear problem without imperfections. Among all these modes, we have selected three: mode $A = \cos(\gamma x)\cos(\beta\gamma y)$; mode $B = \cos(\gamma(1+\beta^2)x)$ and mode $C = \cos(\gamma\beta^2 x)\cos(\beta\gamma y)$, with $\beta = 1.91$ and $\gamma = 0.07$, which corresponds to a number of circumferential waves $n = 15$ for the modes A and C and to the axisymmetric one (mode B) (see Hunt and Neto, 1991).

To make easier the discussion, a specific form of the localized imperfection is chosen as follows:

$$g_1(x,y) = \exp\left(-\left(\frac{x}{C}\right)^2\right)[d_A\cos\gamma x\cos\beta\gamma y + d_B\cos\gamma(1+\beta^2)x + d_C\cos\gamma\beta^2 x\cos\beta\gamma y] \tag{38}$$

where $C > 0$ is the width of the region where the localized imperfection lies and d_A, d_B, d_C are real coefficients linked as $|d_A| + |d_B| + |d_C| = 1$. Nevertheless, according to (37), any shape of localized imperfection is admissible. With the specific choice (38), one obtains analytically the expressions of derivatives of the envelopes in (37). These can be written simply in the form below:

$$\frac{\mathrm{d}a}{\mathrm{d}x}(0) = a_1\delta_A, \quad \frac{\mathrm{d}b}{\mathrm{d}x}(0) = a_1\delta_B, \quad \frac{\mathrm{d}c}{\mathrm{d}x}(0) = a_1\delta_C \tag{39}$$

where a_1 is the imperfection amplitude and δ_A, δ_B and δ_C are given as follows:

$$\delta_A = -\frac{\lambda_c\sqrt{\pi}C}{8k^2(1-\beta^2)^2}\left\{d_A[1+\exp(-\gamma^2C^2)] + d_C\left[\exp\left(-\left(\frac{\gamma(1+\beta^2)C}{2}\right)^2\right) + \exp\left(-\left(\frac{\gamma(1-\beta^2)C}{2}\right)^2\right)\right]\right\} \tag{40}$$

$$\delta_B = -\frac{\lambda_c\sqrt{\pi}C}{8k^2}d_B[1+\exp(-(\gamma(1+\beta^2)C)^2)] \tag{41}$$

$$\delta_C = -\frac{\lambda_c\sqrt{\pi}C}{8k^2(1-\beta^2)^2}\left\{d_A\left[\exp\left(-\left(\frac{\gamma(1+\beta^2)C}{2}\right)^2\right) + \exp\left(-\left(\frac{\gamma(1-\beta^2)C}{2}\right)^2\right)\right] + d_C[1+\exp(-\gamma^2\beta^4C^2)]\right\} \tag{42}$$

Distributed imperfection is considered in the form given by Eq. (32). Influence of this defect on the reduced buckling load is accounted by the right-hand side of the system (29)–(31).

Our aim is to obtain the reduction of the critical load of the compressed cylindrical shell in presence of localized and/or distributed imperfections. For this purpose, we perform a variational formulation and a finite element discretization by using one-dimensional element in x-direction to solve the three ordinary differential equations (29)–(31) with the boundary conditions (39). An iterative algorithm of Newton

Raphson allows us to follow the non-linear branch $\lambda(a, b, c)$ for different values of a_l and a_r. The maximum value of λ is obtained by reading the response curve.

The results obtained by this simplified method are compared with those obtained by using two finite element codes. Now, let us describe how reduced load is computed by using Abaqus. In this analysis we start from a variational formulation of 3D shell mechanics instead of Donnell equations (1) and (2). To compute the load limit for which the collapse occurs, we perform an incremental load–deflection analysis by using the modified Riks method available in Abaqus code.

The buckling mode leads to a displacement pattern with n circumferential waves and m longitudinal ones. The lowest critical load is characterized by specific values of n and m. To predict the critical load, one can model the whole cylinder requiring a fine mesh, but this approach is computationally very expensive. Because of the problem symmetry, we only need to model a part of the shell. Here we shall mesh a half circumferential wave and impose the symmetry conditions. Hence, several analyses are needed to determine which combination (n, m) gives the lowest critical load. Generally, we shall prefer this less expansive analysis than the one involving the whole cylinder discretization.

In our case the critical mode requires 15 waves in the circumferential direction. We then use 10 eight node shell elements in the circumferential direction and 41 elements to model the half cylinder length. So, this mesh involves only 6665 degrees of freedom. On the radial edges, symmetry conditions are imposed and loaded cylinder ends are simply supported. To model correctly the localized imperfection, we meshed finely the middle of the cylinder length (see Figs. 3 and 4). Localized and distributed imperfections are introduced directly in the initial geometry of the shell. To predict a load limit in this way, Abaqus requires about 30 mn CPU time.

Figs. 3–5 describe respectively the modelized mesh, localized and distributed imperfections considered in the present study.

Note that Abaqus has been widely used by the shell buckling research community, see for instance Kim and Kim (2002) and Teng and Song (2001). A convergence study has been presented in Kim and Kim (2002) with the S8R shell element offered in Abaqus. It has been established that accurate solutions, in presence of imperfections, can be obtained with similar meshes as those used in our study.

For completeness, some numerical tests have been also performed with the code INCA (Combescure, 1995), that is based on Fourier series and on one-dimensional finite element. Within INCA, the perfect

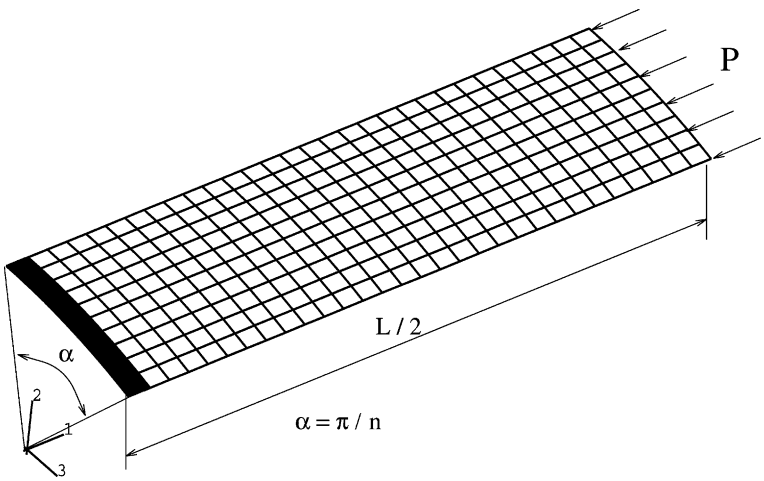

Fig. 3. Description of the modeled geometry and its discretization.

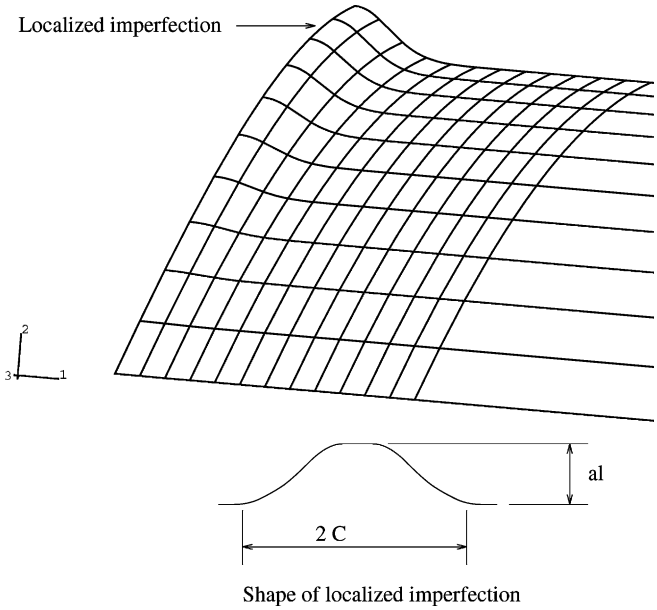

Fig. 4. Meshing and description of the localized imperfection.

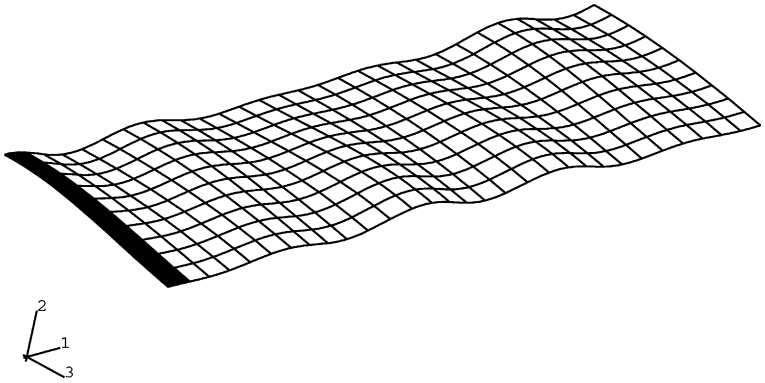

Fig. 5. Description of distributed imperfection.

geometry is discretized, the imperfection is accounted by appropriate terms in the equations as in (1) and (2) and it is expanded into Fourier series. Only four harmonics 0, n, $2n$ and $3n$ will be needed.

4.2. The typical response curve of the axially compressed cylinder

Now we present the typical behaviour of cylindrical shells subjected to an axial compression (Fig. 6). The example chosen for this purpose takes into account only distributed imperfection in the form of Eq. (32) with $d_a = d_b = 1/2$ and $d_c = 0$. Different response curves are then obtained for different values of the amplitude a_r/h. Fig. 6 reporting the load–deflection curves shows that for small values of a_r/h, we have an

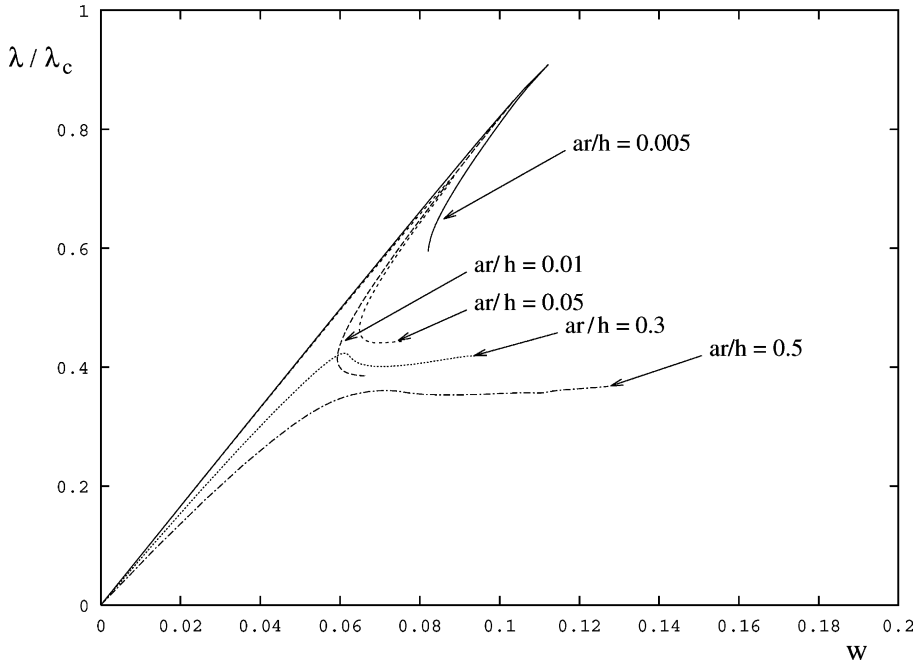

Fig. 6. Load–deflection curves for different perturbation values.

abrupt slope change. This behaviour is smooth for large values of the imperfection amplitude. When a_r is of the order of the thickness, there is no longer load limit and the load–deflection curve is always increasing.

4.3. Influence of localized imperfection

Fig. 7 shows the influence of a localized imperfection. It reports the normalized maximum load λ_{max}/λ_c versus the size of the localized imperfection a_l/h. This imperfection is the one described in Fig. 4 and it is given by Eq. (38) with $C/R = 0.005$ and $d_A = d_B = d_C = 1/3$. A comparison of the results obtained by the proposed method and those given by Abaqus is presented. As an example, for an amplitude of localized imperfection $a_l = h$, we obtain a reduction of 30% for the buckling load ($\lambda_{max}/\lambda_c = 0.7$). The comparative study shows that results given by the simplified method are in agreement with those of Abaqus until a reduction of 40% of the buckling load ($\lambda_{max}/\lambda_c = 0.6$). This analysis shows the great sensitivity of the chosen cylindrical shell to localized imperfections. A localized defect with $C = 0.5$ mm and $a_l = 1.4$ h reduces the critical load of about 40%; that is to say, the imperfect cylinder collapses for a pressure $P_{max} = 0.6P_c = 43.86$ N/mm.

Note that the simplified method is not able to provide accurate results for very small amplitudes of imperfections. Indeed it is known that, in this case, the buckling mechanism is influenced by boundary effects (Yamaki, 1984), that are disregarded in the simplified analysis. To illustrate this phenomenon, we made a calculation with a small imperfection size ($a_l/h = 0.1$). The deformed shape at the ultimate load is presented in Fig. 8 and a post-critical shape in Fig. 9. At the maximal load, two instability mechanisms are present: one sees both a wavy buckle in the region of the localized imperfection and the classical axisymmetric pre-buckling deflection close to the boundary. In the post-buckling range, one recovers about the classical mode without imperfections, that is wavy and focused near boundary.

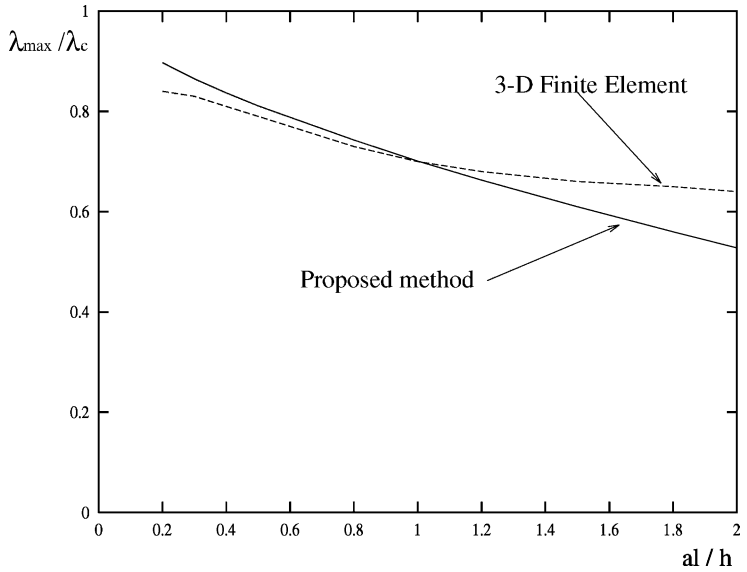

Fig. 7. Localized imperfection: $C/R = 0.005$, $d_A = d_B = d_C = 1/3$.

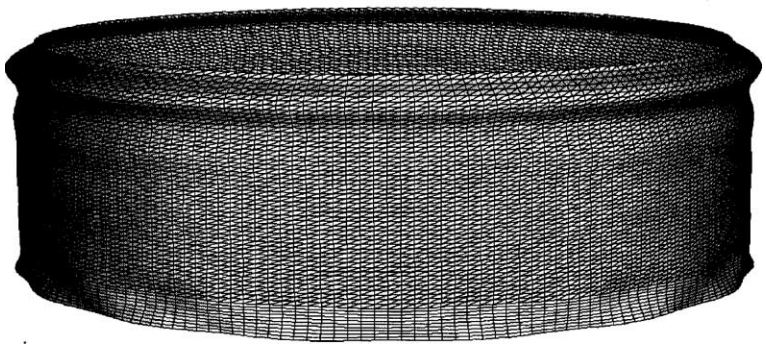

Fig. 8. Deformed shape for the ultimate load. Localized imperfection: $C/R = 0.005$, $d_A = d_B = d_C = 1/3$, $a_1/h = 0.1$.

4.4. Influence of distributed imperfection

In Figs. 10 and 11, we report the influence of only the distributed imperfection geometry on buckling load by plotting λ_{max}/λ_c versus a_r/h. The defect is described in Fig. 5 and given by Eq. (32) with $d_a = d_b = 1/2$ and $d_c = 0$ in the case of Fig. 10 and $d_a = d_b = d_c = 1/3$ in the case of Fig. 11. The comparative study between results obtained by the proposed method and Abaqus is shown on the graphs. In the case of imperfection of Fig. 10 which has no component on mode C, by considering the amplitude $a_r = 0.1$ h, Abaqus predicts a reduction of the critical load $\lambda_{max}/\lambda_c = 0.61$ ($P_{max} = 44.59$ N/mm), and the proposed method gives $\lambda_{max}/\lambda_c = 0.55$ ($P_{max} = 40.21$ N/mm) with a relative error of 10%. For an amplitude $a_r = 0.05$ h, the reduction of the critical load is $\lambda_{max}/\lambda_c = 0.7$ and the relative error is only of about 4%. For a distributed imperfection taking into account three modes, our method gives satisfactory results by comparison with Abaqus until a reduction λ_{max}/λ_c of about 0.7. Discrepancy between the two curves appears for large values of a_r/h.

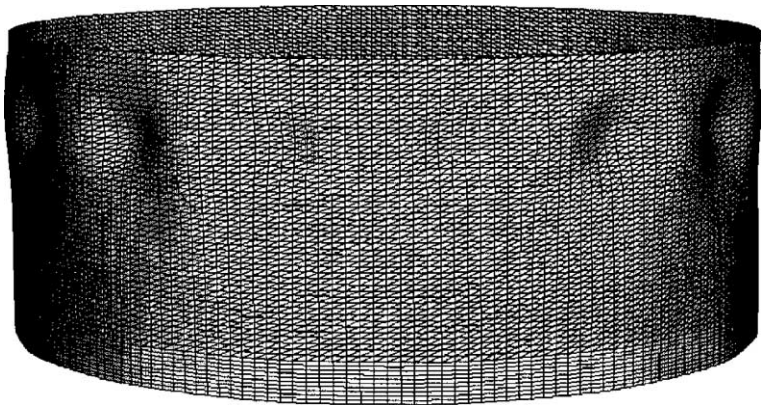

Fig. 9. Deformed shape for the post-critical load $\lambda/\lambda_c = 0.57$. Localized imperfection: $C/R = 0.005$, $d_A = d_B = d_C = 1/3$, $a_1/h = 0.1$.

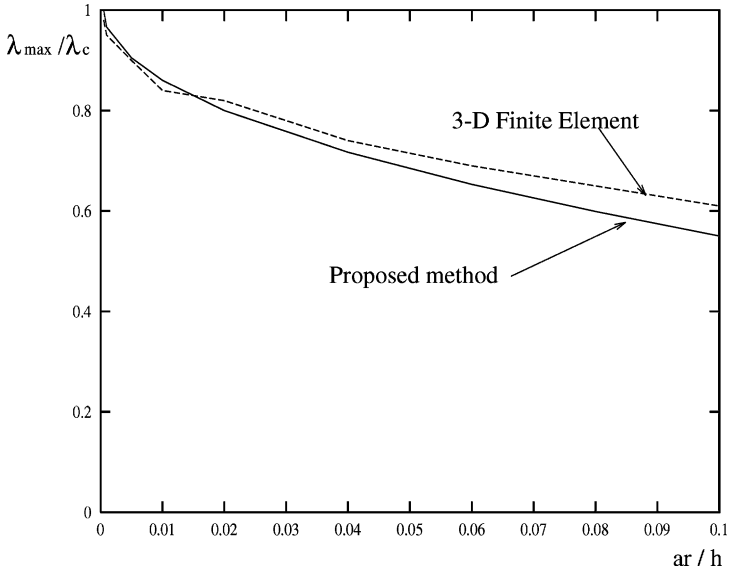

Fig. 10. Distributed imperfection: $d_a = d_b = 1/2$, $d_c = 0$.

For very small amplitudes of imperfections, the reference load–defect curve has a different behaviour according to the type of the imperfection. In a case, the maximum loading tends to the load of Donnell λ_c; in the other case, it tends to a value of about $0.84\lambda_c$, which is in agreement with a bifurcation analysis from a non-linear branch realized by Yamaki (1984). The corresponding modes are represented in Figs. 12 and 13 and they are in coherence with the maximum load obtained. In the case of Fig. 12, we obtain a mode almost axisymmetric and distributed on all the shell: it is similar to those predicted by classical analytical computation leading to Donnell loading $\lambda_c = 1$. In the case of Fig. 13, the mode is periodic ($n = 15$) in the circumferencial direction and, in the axial direction, it is localized near the edges as obtained by Yamaki: note that these instability modes are initiated by circumferential stresses in the neighbourhood of the edges and that for a simply supported cylinder, they reduce the critical load by about 15%. These two curves are different according to the imperfection form, but in the two cases, this imperfection is generic and includes a periodic part. So, in both cases, the technique of following non-linear branches should lead to the lowest

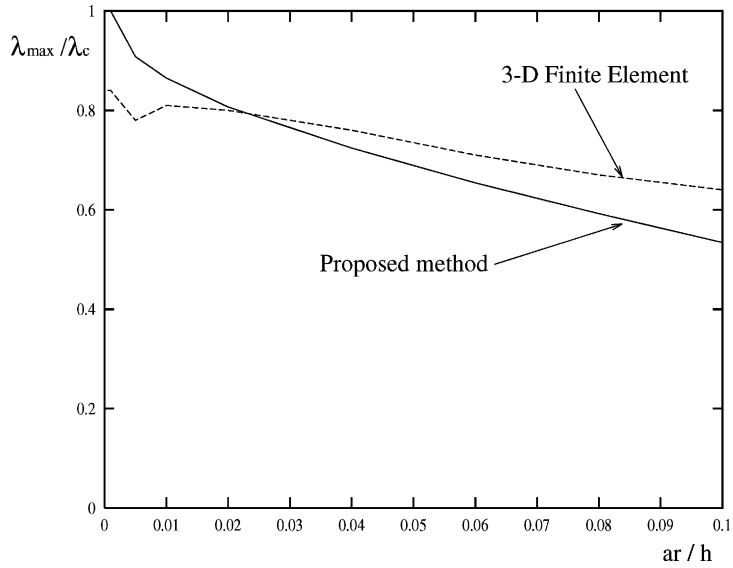

Fig. 11. Distributed imperfection: $d_a = d_b = d_c = 1/3$.

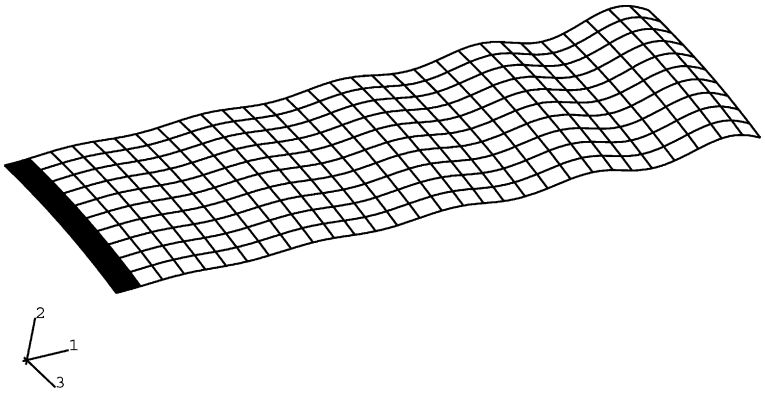

Fig. 12. Deformed configuration, distributed defect: $d_a = d_b = 0.5$, $d_c = 0$, $a_r = 0.0005$, $P_{max}/P_c = 0.985$.

critical load, that is to say to a mode localized near the edges as shown in Fig. 13. The numerical prediction obtained in Fig. 10 is not in conformity with the latter analysis, but remember that there are many coincident modes in the proposed buckling problem and then many solutions branches exist in the studied region: hence, it is not surprising that the computational strategy does not allow us to follow effectively the solution branch for a very small imperfection amplitude. On the other hand, the simplified method proposed in this article gives a value λ_{max} of the order of λ_c for a very small imperfection amplitude that is consistent with the fact that this method does not take into account the effect of boundary conditions.

4.5. Interaction of localized and distributed imperfections

In Fig. 14 the interaction between localized and distributed imperfections is considered. Indeed, we have performed the computation using the following parameters: $d_A = d_B = 1/2$, $d_C = 0$, $d_a = d_b = d_c = 1/3$ and

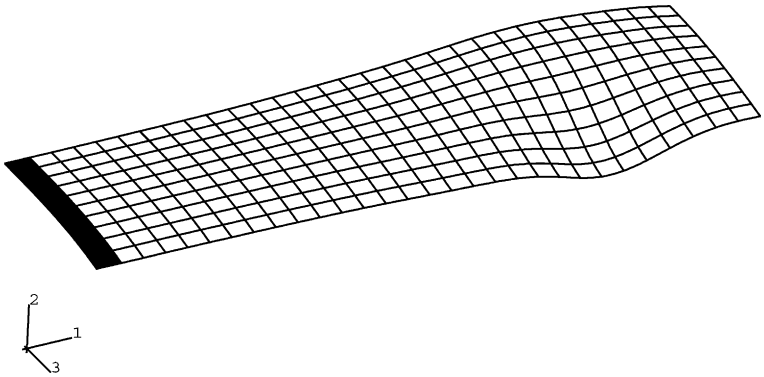

Fig. 13. Deformed configuration, distributed defect: $d_a = 0$, $d_b = d_c = 0.5$, $a_r = 0.0005$, $P_{max}/P_c = 0.840$.

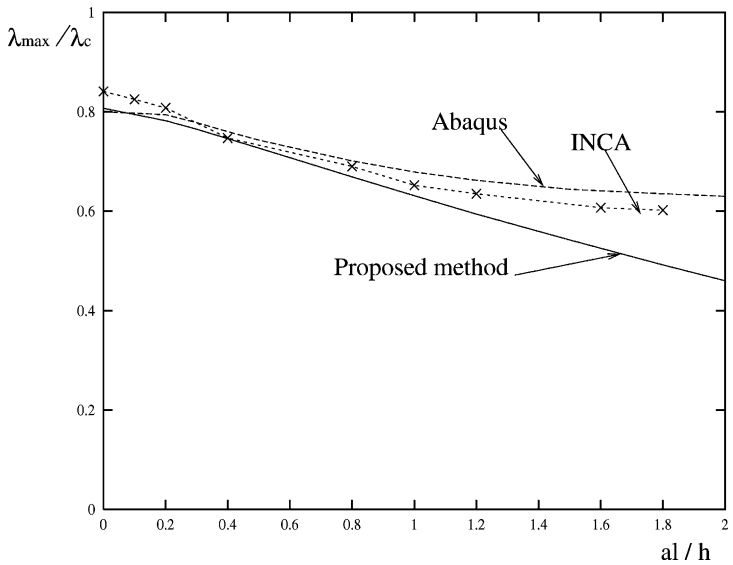

Fig. 14. Interaction of distributed and localized defects: $C/R = 0.005$, $d_A = d_B = 1/2$, $d_C = 0$, $d_a = d_b = d_c = 1/3$, $a_r/h = 0.02$.

$a_r/h = 0.02$. We report in this figure the reduced load λ_{max}/λ_c versus a_l/h for non-zero values of a_r/h. In this case, we have used two reference codes: Abaqus, that is based on three-dimensional shell elements and INCA, that is based on Fourier series and that is specially designed to account for geometric imperfections. There is no significant differences between the two codes (see Fig. 14): this validates the methodology to represent the imperfections in the codes. Note that we have also computed this reduction curve by meshing a half cylinder in height: the results are exactely the same as those obtained by representing a half wave in circumferential direction. Once more, the proposed method gives satisfactory results until a reduction of 30% of the critical load. For a reduction of 40% in the buckling load, a relative discrepancy of about 10% appears between the two methods.

In Fig. 15 are reported several curves by considering the interaction between the two imperfection types. Here only results of the proposed method are drawn. The following parameters are chosen for the computation: $Z = 1000$, $C/R = 0.005$, $d_A = d_B = 1/2$, $d_C = 0$, $d_a = d_b = d_c = 1/3$.

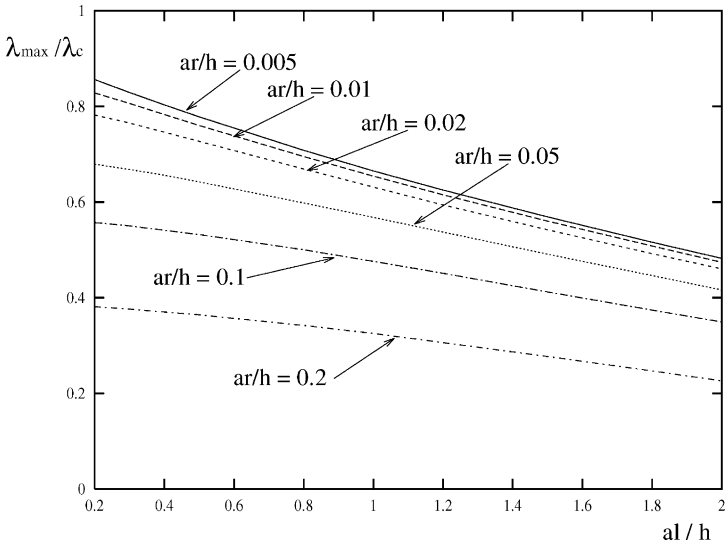

Fig. 15. Interaction of distributed and localized defects: $C/R = 0.005$, $d_A = d_B = 1/2$, $d_C = 0$, $d_a = d_b = d_c = 1/3$.

Let us analyse the interaction between the two types of imperfection by considering an example. When $a_r/h = 0$ and $a_l/h = 1$, only localized imperfection is taken into account, the reduction of the critical load given by the simplified method is $\lambda_{max}/\lambda_c = 0.67$. By considering only distributed imperfection with $a_r/h = 0.02$ and $a_l/h = 0$, the reduction of load is of $\lambda_{max}/\lambda_c = 0.80$. Now, by taking into account the interaction of both localized and distributed imperfections ($a_r/h = 0.02$ and $a_l/h = 1$.), the load reduction is given as $\lambda_{max}/\lambda_c = 0.63$. Hence, a very small distributed imperfection (for instance $a_r/h = 0.02$) has an effective influence, which is what was expected. But this influence is much more significant if this imperfection is alone than if it is combined with a rather large localized imperfection.

For a fixed small value of $a_r/h = 0.005$, curve of Fig. 15 shows a drop in load limit from 0.85 for $a_l/h = 0.2$ to 0.63 for $a_l/h = 1$. That is to say a drop of 25% of the load limit. For a large value of a_r/h, for example 0.1, this drop of load limit is reduced to 14%. Therefore, a given localized imperfection has a stronger influence if it is alone or combined with a small distributed imperfection than if it is combined with a large distributed imperfection.

Therefore, it appears that a given imperfection induces a greater reduction of strength when it is alone that when it is combined with another large imperfection.

5. Conclusions

In this work, we have shown how to take into account the interaction between localized and distributed imperfections by solving a reduced problem deduced from a double scale perturbation technique including three modes interaction. This analysis confirms the great sensitivity of cylindrical shells under axial compression in the presence of both localized and distributed imperfections. The results obtained by the proposed method have been compared with those obtained by classical finite element codes, that are based on various discretization principle. This comparative study establishes that the proposed method gives satisfactory results up to 30–40% of the reduction of the buckling load.

Localized imperfection has a weaker influence on the reduced buckling load by comparison with the distributed imperfection.

Incidentally, a comparison has been performed between a generic three-dimensional shell code and a specific code for shells of revolution. The coherence of the results establishes once more the high reliability of these numerical tools to predict the buckling of imperfect shells.

References

Abdelmoula, R., Damil, N., Potier-Ferry, M., 1992. Influence of distributed and localized imperfections on the buckling of cylindrical shells. Int. J. Solids Struct. 29, 1–25.

Amazigo, J., Budiansky, B., Carrier, G., 1970. Asymptotic analyses of the buckling of imperfect columns on nonlinear elastic foundations. Int. J. Solids Struct. 6, 1341–1356.

Amazigo, J., Fraser, B., 1971. Buckling under external pressure of cylindrical shells with dimple shaped initial imperfection. Int. J. Solids Struct. 7, 883–900.

Arbocz, J., Potier-Ferry, M., Singer, J., Tvergaard, V., 1987. Buckling and post-buckling. In: Lecture Notes in Physics, 288. Springer-Verlag, Heidelberg.

Brush, D., Almroth, B., 1975. Buckling of Bars, Plates and Shells. McGraw-Hill, New York.

Budiansky, B., 1974. Theory of buckling and post-buckling behavior of elastic structures. Adv. Appl. Mech. 14, 1–65.

Budiansky, B., Hutchinson, J., 1966. Dynamic buckling of imperfection sensitive structures. In: Proc. Int. Congr. Appl. Mech., XI. Springer-Verlag, Berlin, pp. 636–651.

Bushnell, D., 1985. Computerized Buckling Analysis of Shells. Martinus Nijhoff Publishers Group.

Combescure, A., 1995. Etude de la stabilité non linéaire géométrique et non linéaire matériau des coques minces. Application aux coques de révolution avec imperfections soumises à des chargements complexes. Habilitation à Diriger des Recherches, INSA de Lyon, France.

Damil, N., Potier-Ferry, M., 1992. Amplitude equation for cellular instability. Dyn. Stab. Syst. 7, 1–34.

Dubas, P., Vandepite, D., 1987. Colloquium on Stability of Plate and Shell Structures. Ghent University Press, Ghent.

Hunt, G., Neto, E.L., 1991. Localized buckling in long axially-loaded cylindrical shells. J. Mech. Phys. Solids 39 (7), 881–894.

Jamal, M., Midani, M., Damil, N., Potier-Ferry, M., 1999. Influence of localized imperfections on the buckling of long cylindrical shells under axial compression. Int. J. Solids Struct. 36, 441–464.

Kim, S., Kim, C., 2002. Buckling strength of the cylindrical shell and tank subjected to axially compressive loads. Thin-Walled Struct. 40 (3), 329–353.

Koiter, W., 1945. On the stability of elastic equilibrium. Ph.D. Thesis, Delf. English translation, NASA Techn. Trans. F10, 1967, p. 883.

Newell, A., Whitehead, J., 1969. Finite band width, finite amplitude convection. J. Fluid Mech. 38, 279–303.

Potier-Ferry, M., 1983. Amplitude modulation, phase modulation and localization of buckling patterns. In: Thompson, J.M.T., Hunt, G.W. (Eds.), Collapse: the Buckling of Structure in Theory and Practice. Cambridge University Press, Cambridge, pp. 148–159.

Potier-Ferry, M., 1987. Foundations of elastic postbuckling theory. In: Lecture Notes in Physics, 288. Springer-Verlag, Heidelberg, pp. 1–82.

Segel, L., 1969. Distant side walls cause slow amplitude modulation of cellular convection. J. Fluid Mech. 38, 203–224.

Teng, J., Song, C., 2001. Numerical models for nonlinear analysis of elastic shells with eigenmode-affine imperfections. Int. J. Solids Struct. 38, 3263–3280.

Thompson, J., Hunt, G., 1973. A General Theory of Elastic Stability. John Wiley, London.

Wesfreid, J., Zaleski, S., 1984. Cellular Structures in Stability Problems.

Yamada, S., Croll, J., 1999. Contributions to understanding the behavior of axially compressed cylinders. J. Appl. Mech. 66, 299–309.

Yamaki, N., 1984. Elastic Stability of Circular Cylindrical Shells. North-Holland, Amsterdam.